Acoustical Imaging and Mechanical Properties of Soft Rock and Marine Sediments (Quarterly Technical Progress Report #15302R05)

Reporting Period: 01/01/02 - 03/31/02

Thurman E. Scott, Jr., Ph.D.
Younane Abousleiman, Ph.D.
Musharraf Zaman, Ph.D., P.E.

Report Issued: April 30, 2002

DOE Award Number: DE-FC26-01BC15302

Rock Mechanics Institute
The University of Oklahoma
Sarkeys Energy Center, Room P-119
100 East Boyd Street
Norman, Oklahoma 73019-1014

DISCLAIMER

ABSTRACT

Three major goals were accomplished during this phase. First, a study was completed of the effects of stress-induced changes in anisotropic elastic moduli in sandstone. Second, a new method for measuring the anisotropic poroelastic moduli from acoustic data was developed. Third, a series of triaxial experiments were conducted on unconsolidated sands to identify pressure/stress conditions where liquefaction occurs under high confining pressures. Stress-induced changes in anisotropic Young's moduli and shear moduli were observed during deformational pathway experiments. A new method was made for the acquisition of compressional and shear wave velocities along a series of 3-dimensional raypaths through a core sample as it is subjected to deformation. Three different deformational pathway experiments were conducted. During the hydrostatic deformation experiment, little or no anisotropy was observed in either the Young's moduli or shear moduli. Significant deformational anisotropies were observed in both moduli during the uniaxial strain test and the triaxial compression experiment but each had a different nature. During the triaxial experiment the axial and lateral Young's moduli and shear moduli continued to diverge as load was applied. During the uniaxial strain experiment the anisotropy was `locked in' early in the loading phase but then remained steady as both the confining pressure and axial stress were applied. A new method for measuring anisotropic Biot's effective stress parameters has also been developed. The method involves measuring the compressional and shear wave velocities in the aforementioned acoustic velocity experiments while varying stress paths. For a stress-induced transversely isotropic medium the acoustic velocity data are utilized to calculate the five independent elastic stiffness components. Once the elastic stiffness components are determined these can be used to calculate the anisotropic Biot's effective stress parameters, α_v and α_h, using the equations of Abousleiman et al. (1996). A series of experiments have been conducted, on an initially inherently isotropic Berea sandstone rock sample, to dynamically determine these anisotropic Biot's parameters during deformational pathway experiments. Data acquired during hydrostatic, triaxial, and uniaxial strain pathway experiments indicates that Biot's effective stress parameter changes significantly if the applied stresses are not hydrostatic. Variations, as large as 20% between the axial (vertical) and lateral (horizontal) Biot's effective stress parameters, were observed in some experiments. A series of triaxial compression experiments have been conducted on unconsolidated sand (Oil Creek sand) to determine the pressure/stress conditions which would be favorable for liquefaction. Liquefaction of geopressured sands is thought to be one of the major causative mechanisms of damaging shallow water flows. The experiments were developed to determine if: (1) liquefaction could be made to occur in this particular sand at high confining pressures, and (2) the state of liquefication had the same nature at high pressure conditions typical of shallow water flows as it does in low confining pressure soil mechanics tests. A series of undrained triaxial experiments were successfully used to document that the Oil Creek sand could undergo liquefaction. The nature (i.e., the shape of the deformational pathway in mean pressure/shear stress space) was very similar to those observed in soil mechanics experiments. The undrained triaxial experiments also indicated that this sand would strain soften at relatively high confining pressures – a necessary precursor to liquefaction. These experiments serve as a starting point for a series of acoustic experiments to determine the signature of compressional and shear wave properties as the sand packs approach the state of liquefaction (and shallow water flows).

TABLE OF CONTENTS

LIST OF GRAPHICAL MATERIALS FOR THE PROJECT

EXECUTIVE SUMMARY

Two major experimental developments were completed in this phase of the project and papers on each were submitted for publication in the 2nd Biot Conference on Poromechanics to be held in Grenoble, France on August 26-28, 2002. The first paper is entitled "Determination of the Stress-induced Dynamic Moduli of a Porous Medium Subjected to Various Deformational Pathways" by T.E. Scott, Jr. and Y. Abousleiman. The second paper is entitled "An Experimental Method for Measuring Anisotropic Poroelastic Biot's Effective Stress Parameters from Acoustic Wave Propagation." The basic text of both papers is included in this progress report. These deal with the role of stress-induced anisotropy on both elastic and poroelastic parameters. The role of inherent anisotropy, that is the anisotropy associated with sedimentary features such as bedding or structural features such a fractures, have been well studied. However, the role of stress-induced anisotropy has not been examined. Previous research, measuring axial and lateral compressional and shear wave velocities during triaxial rock deformational experiments, indicates that a significant velocity anisotropy will develop as stress-induced deformation intensifies. However, the effect of this stress induced velocity change cannot be easily translated into a calculation of anisotropic elastic parameters unless off-axis velocity measurements are obtained to accompany the axial and lateral acoustic raypaths. The anisotropic elastic parameters are being increasingly required for engineering studies (such as for borehole stability). For the first time, we have developed a new method for measuring both the axial, lateral, and off-axis compressional and shear wave velocity components needed to determine the magnitudes of stress-induced anisotropy on porous rocks. This method was used to obtain data on the anisotropy developed in axial and lateral Young's moduli and shear moduli in sandstone during different deformational pathways. During the hydrostatic pathway, where equal stresses are increased, the sandstone sample did not show evidence of the development of anisotropy. However, during triaxial and during uniaxial strain experiments a significant anisotropy, in both the Young's moduli and shear moduli were evidenced. During the triaxial experiment the anisotropy developed early in the loading phase and continued to increase as axial stress was applied while maintaining the confining pressure constant. During the uniaxial strain experiment, the anisotropy developed early in the loading phase but after a short displacement this initial stress-induced anisotropy was 'locked in' and maintained as axial stress was increased. The second part of this same study involved examining the stress effects on the anisotropic Biot's effective stress parameters. In research we utilize the new experimental method to obtain the stiffness components of the anisotropic medium and then show a new way to calculate the anisotropic Biot's effective stress parameters. The results indicate that anisotropic stress will generate significant changes in the poroelastic rock parameters as well.

Work during this quarter also involved making a series of undrained triaxial compression tests on Oil Creek sand. Experimental methods were developed so unconsolidated sands could be tested at high confining pressures under conditions simulating those where shallow water flows occur in the marine environment. The results indicate that liquefaction can occur in this type of sand deformed at high confining pressures. Liquefaction, the runaway instability where sand flows uncontrollably, is thought to be a major component in the devleopment of shallow water flows which are so damaging to deep water drilling operations. This successful series of undrained experiments are intended to be reconnaissance tests for velocity experiments which are now being conducted that utilize the new technologies described above.

Determination of the Stress-induced Dynamic Moduli of a Porous Medium Subjected to Various Deformational Pathways

The state of stress in the shallow crustal environment is distinctly anisotropic. Typically, the vertical stress and the horizontal stress are not equal. In many sedimentary basins, which do not have large tectonic stresses superimposed on them, the vertical stress is much greater than the horizontal stresses. For example, Nelson (1981), notes that in the U.S. the ratio of the horizontal to vertical stresses can be as low as 0.2. The stress state must be accounted for when evaluating engineering problems such as borehole stability. The effect of stress-induced anisotropy on elastic/poroelastic parameters has not been investigated. Experimentally it has been well documented that stress induced anisotropy does affect the development of both compressional and shear wave velocities (Nur and Simmons 1969; Fjaer et al. 1989; Sayers and van Munster 1991; Wu et al. 1990; Scott et al. 1993). So it could be surmised, based on those studies, that the elastic moduli would exhibit an anisotropy. However these studies measured the velocities in only the axial and lateral directions of the cores during triaxial deformation. In these cases the acoustic data are insufficient to allow a calculation of the anisotropic elastic moduli. In this study we develop a method for measuring the effects of stress induced anisotropy on a variety of elastic parameters (including the anisotropic Young's moduli, E_v and E_h, and the anisotropic shear moduli G_h and G_v) during different deformational stress pathways.

Dynamic methods involving the acquisition of compressional and wave velocities have long been used to document the inherent anisotropy of rocks (Podio et al. 1968; King 1969; Jones and Wang 1981; Lo et al. 1986; King et al. 1994). Inherent anisotropy results from natural features in rocks such as bedding planes, layering, or fracturing. Most researchers examining inherent rock anisotropy, utilize the 'three oriented core' method to acquire data on rocks they assume will exhibit a transverse isotropy. In this method oriented plugs are cut (generally 0^o, 90^o, and 45^o to bedding) from a rock sample and then the acoustic compressional and shear wave velocities are measured along the axis of each of the oriented plugs. The compressional and shear wave velocity then are used to calculate the components of the stiffness matrix including C11, C13, C12, C13, and C44 which are the five independent constants needed to define a transversely isotropic rock (King 1969). The stiffness parameters require an 'off-axis' compressional raypath to calculate the C_{13} stiffness component (generally this is oriented at 45^o). If these data are obtained then the dynamic anisotropic elastic moduli including Young's moduli (E_v, E_h), and the shear moduli (G_v, G_h) can be calculated (King 1969 for details).

As previously noted much data has been obtained on inherent anisotropy of elastic parameters using this `three oriented core' approach. The three oriented core method, however, is not suitable to examine the effects of non-hydrostatic deformational states of stress on inducing anisotropy in rocks. For example, if the rock is initially isotropic and a stress induced anisotropy is elastically created then axial measurements (either dynamic or quasistatic) on a core are insufficient to describe it. Rotating the core will not allow access to the lateral parameters of the core in the stress induced case as it does for the inherent anisotropy.

The use of a single core with an array of compressional and shear wave acoustic sensors mounted around the sample represents the most attractive method for overcoming the limitations of the three core method. The single core method has been used recently to examine anisotropy in Biot's effective stress parameters (Scott and Abousleiman 2001) and inherent anisotropy (Wang 2001) under hydrostatic conditions. In this study the technique is developed for use to examine the effects of stress induced anisotropy in a triaxial pressure cell.

The Berea sandstone core samples made for the study were 15 cm long and 7.6 cm in diameter. Three deformational pathway experiments were conducted in an MTS 315 load frame with a 140 MPa

triaxial cell. The first test was a hydrostatic compression test where the confining fluid pressure around the rock was raised. The triaxial compression experiment was conducted by axially loading the sample while a confining pressure of 20 MPa was maintained around the sample. A uniaxial strain experiment was conducted in the third test where the lateral strain was maintained at near zero while both the confining pressure and axial stress were increased. During each experiment a total of 11 acoustic raypaths were acquired on a right circular cylinder (Figure1). The raypaths included V_{P33}, V_{P22}, V_{P11}, V_{S31}, V_{S32}, V_{S12}, V_{S13}, V_{S32}, V_{S23}, $V_{P45(1\text{-}3a)}$, and $V_{P45(1\text{-}3b)}$. The 3 direction is parallel to the axis of the core and the 2 and 1 direction are the lateral directions, respectively. If a transverse isotropic condition can be documented then only five of these velocities are needed to complete the calculations. In our study we use the V_{P33} (the axial compressional wave), V_{P22}, (the lateral compressional wave), $V_{P45(1\text{-}3a)}$ (one of the compressional waves in the 1-3 plane oriented at 45^{o} to the core axis), Vs_{31}, (the vertically propagating shear wave polarized in the 1-3 plane), and the horizontally propagating shear wave (V_{s12}) polarized in the horizontal (1-2) plane (Figure 2). The additional waves are not used in the calculations but are, in fact, necessary to document the fact that only a transverse isotropy was developed in such a rock. The axial compressional and shear wave elements are housed in the steel loading platens and the lateral sensors are glued directly to the outside of the rock sample.

The Berea sandstone block selected for the study was very uniform and had no discernable bedding plane fabrics or observable anisotropy or inhomogeneities. The initial porosity was 23%. In the course of selecting our starting material it was discovered that different Berea blocks exhibit significant variability in both homogeneity and inherent anisotropy. Three-dimensional compressional wave velocity measurements were used to insure that the block selected for the study had a minimal anisotropy.

Figures 3a and 3b show the stress-strain curve and the axial and lateral dynamic Young's moduli from the hydrostatic experiment. During this experiment the fluid confining pressure was raised up to 60 MPa. The initial Young's moduli was 16 GPa but increased up to 27 GPa at the termination of the experiment. The shear moduli (Figure 3c) shows an initial rapid increase as pressure is applied and then achieves a steady-state nature around 20 MPa confining pressure after which very little change occurs. During this experiment there was no significant anisotropy developed in either the shear moduli or the Young's moduli.

A triaxial experiment was conducted at 20 MPa confining pressure (Figure 4a). This sample was only loaded to 100 MPa to confine the measurements to the elastic range (previous work on different blocks of Berea (Scott et al. 1993) indicated that failure would occur at 150 MPa and that significant dilatant anisotropy would be developed above 100 MPa). The initial axial and lateral Young's moduli were equal (around 24 GPa) but as loading was increased a significant anisotropy developed. The axial (vertical) Young's modulus (E_v) increased whereas the lateral (horizontal) Young's modulus (E_h) decreased (Figure 4b). The shear moduli also exhibit an anisotropy which increases as axial load is applied. In this case there is a larger decrease in the shear modulus within the plane of isotropy (G_h) than in the vertically oriented shear modulus (G_v) (Figure 4c).

The uniaxial strain experiment also exhibited the development of an anisotropy in both the Young's moduli and the shear moduli but with an entirely different nature (Figures 5a, 5b, 5c). In this experiment both the confining pressure and axial stress are increased together while maintaining the near zero lateral strain condition (to within .00001 strain). As deformation proceeds both the Young's moduli and shear moduli show initial increases. After about 10 MPa differential stress the anisotropy, which developed early, seems to be 'locked in' and thereafter shows little or no change even though both axial and lateral stresses are increasing.

The development of a stressed induced anisotropy in rock samples in the elastic moduli has long been suspected and deduced from data on compressional and shear wave data during deformation experiments (e.g., Nur and Simmons 1969; Fjaer et al. 1989; Scott et al. 1993). In this study, a method was developed to allow the actual values of the anisotropic elastic Young's moduli

and shear moduli to be measured and calculated. These data can then be incorporated into engineering programs analyzing problems such as borehole stability.

The anisotropies developed during the hydrostatic, triaxial, and uniaxial strain experiments are all different. The hydrostatic experiment exhibited little or no anisotropy as confining pressure was increased (just as was observed by Lo et al. 1986). During the triaxial and uniaxial strain experiments, those in which the axial and lateral stresses were different, did exhibit a significant anisotropy. In the case of the triaxial experiment anisotropy in the Young's modulus was significant (30 GPa for the axial case and 20 GPa) for the lateral case at termination of the experiment). In the case of the uniaxial experiment the anisotropy was lower (25 and 20 GPa for the axial and lateral respectively) but still significant.

These results suggest that stress induced anisotropy in the elastic moduli of rocks can be significant. The new experimental method will be used in the future to examine stress-induced changes in the moduli of different rock types with varying porosities.

An Experimental Method for Measuring Anisotropic Poroelastic Biot's Effective Stress Parameters from Acoustic Wave Propagation

The Biot's effective stress coefficient, α, is very important in a wide range of engineering problems ranging from borehole stability and fault–reactivation, to reservoir compaction. This coefficient corrects the fluid pressure component (p) in the effective stress law (Biot and Willis 1957; Thompson and Willis 1991):

$$\sigma'_{ij} = \sigma_{ij} + \alpha_{ij} p$$

For a homogeneous, isotropic medium, Biot's effective stress coefficient can be determined using a quasi-static approach by subjecting a fluid saturated porous rock to a stress perturbation under hydrostatic state of stress. Generally it is accomplished by two experimental methods: the direct and indirect method. The indirect method involves measuring the bulk modulus of the solid grains (K_s) during a drained unjacketed hydrostatic test, and the bulk modulus of the rock grain framework (K) during a jacketed drained hydrostatic test. Biot's parameter can then be calculated as $\alpha=1-K/K_s$. The direct method involves determining the ratio between the pore fluid volume change to the total bulk volume change during deformation. Biot's coefficient has been determined using these methods for a wide range of rock types with typical values ranging from 0.3 to 1 (Fatt 1959; Abousleiman and Ghassemi 1992; Abousleiman et al. 1994; Laurent et al. 1993; Fabre and Gustkiewiez 1998; Franquet and Abass 1999). It is important to note that both of these methods involve quasi-static measurements of volumetric properties (i.e., bulk total volume or pore fluid volume) and not directional properties.

The theory for poroelastic anisotropy with Biot's effective stress parameter, α_{ij}, has been developed theoretically (Biot and Willis 1957; Carroll 1979; Thompson and Willis 1991; Abousleiman and Cheng 1993; Abousleiman and Cheng 1996; Cheng 1997; Abousleiman and Cui 2001). In this case the Biot's parameters develop a directional nature. Rock anisotropy can be subdivided into two types: (1) inherent anisotropy in rock due to natural features (such as layering, bedding, etc.) and (2) stress induced anisotropy resulting from deformation of the rock in a non-hydrostatic state of stress. A knowledge of both is important for application to engineering problems. Attempts have been made to determine inherent anisotropic poroelastic parameters. These use variations of the oriented three plug method (see Aoki et al. 1993 for the

use of this method) while applying the above noted quasi-static indirect or direct methods to determine inherent anisotropic Biot's parameters.

The application of quasi-static methods to measure stress-induced poroelastic parameters presents the experimentalist with severe technical problems. The three oriented-core quasi-static method involves the measurement of volumetric properties which cannot lend itself to a determination of the directional properties needed for stress-induced anisotropic Biot's parameters. As noted by Scott and Abousleiman (2002) the superposition of a triaxial state of stress ($\sigma_3>\sigma_2=\sigma_1$) on an initially inherent isotropic rock will result in the development of a stress-induced isotropy in the rock. In such cases reorienting an initial isotropic rock within a stress field while measuring volumetric properties simply results in redundant measurements. A new method using the directionality of acoustic wave propagation seemed the most promising route to circumvent the problems associated with the quasi-static methods.

The main question of the study is to discern if anisotropic stresses applied to an inherently isotropic rock will affect the Biot's effective stress parameters. Available data on subsurface stresses suggested that the state of stress is not isotropic. For example, Nelson (1981) in his review noted very significant variations in the horizontal to vertical stresses in many geological environments. For example, in the U.S. the ratio of the horizontal to vertical stresses can vary by as much as 0.2. If subsurface stresses are generally non-hydrostatic then it could be surmised that the Biot's effective stress parameters may also exhibit some form of anisotropy.

Given the importance of both inherent and stress-induced anisotropy in rocks it would be valuable to determine some way to measure the anisotropic Biot's parameters in either or both cases. Scott and Abousleiman (2001) suggested that the technical problems associated with utilizing the quasi-static methods could be overcome by using dynamic methods to determine the stiffness components of the anisotropic Biot's parameters derived by Abousleiman and Cheng (1993). Abousleiman et al. (1996) and Cheng (1997) expressed the anisotropic Biot's parameters in terms of the elastic stiffness constants. In the case of a general anisotropy the Biot's effective stress parameters can be described as:

$$\alpha_{ij} = \delta_{ij} - \frac{C_{ijkk}}{3K_s}$$

where K_s is bulk modulus of the solid grains (Abouseliman and Cheng 1993; Cheng 1997).

For a transversely isotropic material (Abousleiman et al. 1996):

$$\alpha_h = 1 - \frac{C_{11} + C_{12} + C_{13}}{3K_s}$$

$$\alpha_v = 1 - \frac{2C_{13} + C_{33}}{3K_s}$$

Where α_v is the vertical Biot's parameter paralleling the axis of symmetry and α_h is the horizontal Biot's parameter in the plane of symmetry for a tranversely isotropic rock. Dynamic methods can be used to determine the stiffness components allowing the anisotropic Biot's effective stress parameters to be calculated. The use of compressional and shear wave velocities along multiple raypaths propagated through anisotropic samples has been utilized by researchers to determine inherent anisotropic elastic properties (King, 1969; Lo et al., 1986). For example many

researchers have used dynamic methods to determine the inherent anisotropic Young's modulus, shear moduli, and Poisson's ratios for various rocks. It should be noted that the new method does require an independent separate experiment to determine the solid grain bulk modulus (i.e., a unjacketed, drained hydrostatic test) and the assumption of microisotropy (Abouseilman et al. 1996; Cheng 1997; Abousleiman and Cui 2001).

During the hydrostatic compression test (Figures 6a and 6b) the Biot's parameters show a decrease as confining pressure is increased. Initial values, at 20 MPa, in α_{ϖ} are .83 and α_h are .80, respectively. These decrease rapidly as pressure is applied and achieve a steady state nature around .6. At the termination of the experiment (60 MPa), α_h was .62 and α_v was .58. The values of Biot's parameters are consistant with those obtained for Berea sandstone quasi-statically during hydrostatic (isotropic) compression experiments (Abousleiman et al. 1994). As confining stress is increased the rock framework becomes much stiffer (i.e., the bulk modulus, K, of the framework increases) as grain-to-grain contacts are closed and the pore spaces are compressed. Since:

$$\alpha = 1 - \frac{K}{K_s}$$

a decrease in Biot's parameters is observed. (Note that K_s was measured in a separate experiment at 37 GPa. During the hydrostatic experiment a very slight anisotropy was observed in the values of the axial and lateral Biot's parameters but the values do track each other as stress is applied.

In contrast there was a stress induced anisotropy built up during the triaxial compression experiment at 20 MPa confining pressure (Figures 7a and 7b). During this experiment the differential stress was not allowed to exceed 100 MPa during loading so that the velocity data would primarily reflect elastic deformation. Previous triaxial tests on this rock (Scott et al. 1993) indicated that failure would occur around 150 MPa. During this experiment the Biot's parameter in the lateral direction, a_h , showed an increase from .70 to .76 as deformation proceeded. The axial lateral Biot's parameter, a_v, showed very little change (a slight decrease from .70 to .67). In this experiment there was an anisotropy developed as deformation was applied to the sample (Figure 7b). Figures 8a and 8b show the changes in the anisotropic Biot's parameters during a uniaxial strain experiment. In this experiment an initial confining pressure of 6.9 MPa was applied to the sample before initiating the uniaxial strain condition. During this experiment the lateral Biot's parameter, α_h, decreased from .75 to .65 whereas the axial Biot's parameter, α_v, decreased from .77 to .54 as deformation increased. There was a significant anisotropy developed between the axial and lateral Biot's parameters (Figure 8b). This anisotropy developed very early in the experiment but at about 20 MPa confining pressure the anisotropy seemed to be `locked in' and little or no change in the magnitudes of either the Biot's parameters or the anisotropy was observed.

The results of the hydrostatic experiment seem straightforward. During the application of an isotropic state of stress the Biot's parameter decreases as the rock framework becomes stiffer and very little anisotropy between the axial and lateral directions in the sample was observed. In comparison the experiments involving an application of triaxial states of stress (the triaxial compression test at constant confining pressure and the uniaxial strain test at constant lateral strain) show the development of a marked anisotropy in the axial and lateral Biot's parameters as deformation is increased. The magnitude of the anisotropy, particularly in the case of the uniaxial strain experiment, is significant. These laboratory results suggest stress induced anisotropic variations in Biot's parameters may also be important in the natural setting as

anisotropic states of stress in the subsurface are the normal state. As previously noted, Nelson (1981) highlighted cases in the where the ratio of horizontal to vertical stresses were on the order of 0.2.

Of the three tests conducted in this research study the experiment that best simulates subsurface stress state would be the uniaxial strain experiment. In that experiment both the axial and lateral stresses are changed as deformation proceeds. This experiment illustrated the most change in the magnitude (20%) of the anisotropy in the Biot's effective stress parameters.

Shallow Water Flows

Shallow water flows are the uncontrolled flow of unconsolidated sands and pore water that occur in oil and gas drilling operations in the marine environment. They generally occur at shallow depths below the seafloor (less than 2000 feet) but in deep water (2000-4000 feet). They were first identified in 1985 in the Gulf Mexico Coast (Faul et al. 2000). Shallow water flows are marked by a variety of seafloor damage including: (1) uncontrolled flow of sand up and around the annulus of the borehole being drilled; (2) sand and pore fluid 'volcanoes' on the seafloor near the drill site; (3) craters on the seafloor; (4) borehole washouts; (5) cracks on the seafloor (Alberty 2000; Faul et al. 2000). All are testament to the dynamic nature of this geotechnical phenomenon. Shallow water flows are a major financial problem for the oil and gas industry working in deep water. An industry analysis of the severity of the problem indicated that the industry had lost 175 million dollars on 106 wells for an average of 1.6 million dollars per well since the problem was discovered (Alberty 2000). The flows of these sands can be so severe that they can lead to loss of the surface casing, loss of drilling templates and abandonment of the oil gas production. The loss of the multiwell URSA development project in Mississippi Canyon Block 810 was an example of the loss the industry suffered when violent shallow water flows damaged the facility (Furlow 1998).

Shallow water flows occur in unconsolidated, geopressured sand sections. The industry is trying to deal with the problem via two methods. The first involves engineering approaches to solve shallow water flows after they have occurred. These include: (1) using foam cements to seal off flow; (2) drilling the well with weighted drilling mud; (3) drilling with oversized risers; (4) drilling with rotating BOPs with dual gradient drilling muds; (5) hydraulic isolation using external packers; and (6) hydraulic isolation using annular shutoff seals and valves (Alberty 2000). None of these engineering solutions has been successful enough to gain widespread industry acceptance. The second solution to shallow flows is to seismically predrill detect potential zones thereby assessing the hazard potential of a given site and sidestepping a location that would be potentially problematic. Shallow water flows are thought to originate from geopressured sand sections that have been sealed off by surrounding shale formations. They occur in sedimentological features such as channel sands and buried submarine slumps or debris flows (McConnell 2000). Identification of sand formations that could generate shallow water flows involves trying to directly seismically detect either the overlying shale sealing units or the geopressured sand (McConnell 2000; Huffman and Castagna 2000). Advanced technologies such as 3-D seismic surveying are now in use to try to detect these zones (McConnell and Campbell 1999). Most companies utilize reprocessed marine hazard seismic surveys in an attempt to detect problem zones. There are two factors of primary interest concerning sands that yield shallow water flows. Geophysicists are interested in the Vp/Vs ratios of the geopressured sands for predrill detection. Engineers are interested in the shear strength of the sands (which indicates the degree of weakness of the formation).

The experimental program in this study is designed to address both of these issues. In this phase of the study we tried to determine: (1) the best experimental procedures for conducting triaxial tests on weak sands at high pressures; and (2) the pressure/stress conditions, best approximating the conditions observed in the deep water marine environment, where

liquefaction in unconsolidated sands would occur. With that in mind a series of undrained triaxial compression tests have been used to outline the conditions where liquefaction, and therefore, shallow water flows would occur.

Liquefaction

Liquefaction results from the strain-softening of a saturated soil or sand sample (Vaid and Eliadorani, 1998). The process results in the rapid, catastrophic flowing of sand and has been responsible for the failure of many engineering structures such as dams – e.g., the Fort Peck and San Fernando Dams (Vaid and Eliadorani 1998). Liquefaction is also a major problem in loose soils when earthquake shocks occur. Huffman and Castagna (2000) have noted that shallow water flows may be caused by liquefaction. The similarities are striking. First, the sands are uncontrollably flowing and they occur in precisely the same conditions (e.g., high pore fluid pressures and loose sands) where liquefaction is favored. Second, they have the appearance of flowing sand that is characteristic of liquefaction.

The study of the process of liquefaction has primarily been the province of civil engineers who have extensively examined the process during static (i.e., triaxial) and dynamic (i.e., cyclic) experiments. Generally this research has been conducted at relatively low confining pressures (0-100 psi). As previously noted shallow water flow problems occur in deep water (2000-4000 feet) but at relatively shallow depths below the mudline (0 to 2000 feet). Under these conditions experiments at high confining pressures may be more appropriate than those conducted for soil mechanics experiments.

Liquefaction has been identified to occur under a specific set of stress conditions. Figure 9 shows a schematic of two undrained tests to show the two very different undrained deformational responses of a weak sand. An experiment at low effective confining pressure, as seen by pathway a-f-g-h in Figure 9 does not develop any instability. After an initial hydrostatic deformation (part a-f) the sample undergoes axial loading (f-g). At point F the sample yields and begins to work harden until it stops on the critical state line. The critical state in soil mechanics is defined as the point were the sample continues to deform with no change in volume (Schofield and Wroth 1968). No instability, or strain softening, will be observed in this type of sample.

A triaxial undrained experiment at much higher confining pressure (pathway a-b-c-d-e) illustrates a much different behavior. This is a pathway which will develop an instability typically associated with liquefaction. The hydrostatic portion is from a-b. As axial loading is applied the sample develops a significant pore pressure which reduces the effective mean pressure on the sample. At point c of this deformational path the sand begins to weaken. The unstable portion of the path occurs from point c to d. If the experiment is conducted under stroke (displacement) control the experiment will soften and no violent instability will occur. However, if it is under load control the sample will rapidly deform as the servo-control system tries to maintain successively higher stresses. This violent instability is the hallmark of liquefaction in the natural setting. It is also thought to be the causative mechanism for shallow water flows.

A series of undrained triaxial tests have been conducted to outline, for the Oil Creek sand, the conditions where these instabilities occur. This sand is very clean (99.9% quartz) and the grains are well rounded with grain sizes which average around .2mm. These tests were on NX, size samples during which the axial and lateral strains and pore pressure changes were monitored as deformation proceeded. Figures 10 and 11 show the preliminary results of a comparison of two triaxial undrained tests on the Oil Creek sand. Three plots are used to define each experiment. The first diagram plots the axial stress-strain curve. The second plots the effective

mean pressure versus shear stress. The third diagram plots the pore pressure evolution versus shear stress. These experiments were conducted at a constant axial deformation rate of .005 in./min. After the initial hydrostatic loading was completed the "B" value was checked (i.e., Skempton's parameter) to insure that the sample was 100% water saturated. The B value is the ratio of the pore pressure to confining pressure as change confining pressure is increased. A value of 1 in an unconsolidated sample generally indicates the sample is fully saturated.

These two sets of data represent just two runs out of several dozen that were conducted to locate the conditions where the Oil Creek sand undergoes liquefaction. These two were selected because they are most closely representative of the two pathways outlined in Figure 9.

The undrained experiment at 2000 psi confining pressure and 1000 psi pore fluid pressure is shown in Figures 10a, 10b, and 10c. The stress-strain curve for this sand exhibits an initial linear elastic section until a differential stress of 750 psi is attained (Figure 10a). After that point the sample exhibits a work hardening stress-strain curve up to about 16% percent axial strain after which it exhibits a steady-state nature. Figure 10c shows the evolution of the pore fluid pressure during the experiment. Initially, the pore pressure increases (during the elastic loading phase) and then begins to decrease. The stress-strain curve work hardens as deformation continues until the critical state is achieved. The critical state in soil mechanics is defined as the point were the sample continues to deform with no change in volume (Schofield and Wroth, 1968). It is important to note that no instability, or strain softening, was observed in this sand sample. Evidence that the critical state has been achieved is that the effective stress condition (point a in Figure 10b) and the pore pressure (point b in Figure 10c) are 'locked in' while the sample continues to deform (strain path from c to d in Figure 10a).

The undrained experiment at 5500 psi confining pressure and 600 psi pore pressure exhibits a very different behavior. This triaxial experiment is equivalent to the idealized pathway at higher effective mean stress in Figure 9. The stress-strain curve shows an initial elastic portion (up to 1% axial strain) and then evidences a slight strain softening (Figure 11a). At about 6% axial strain the sample begins work hardening. Both of the the two triaxial experiments described in this section were conducted under stroke control. If the sample had been conducted under load control the strain softening portion of the stress-strain curve would be a 'runaway' instability which would be equivalent to liquefaction. The weakening of the sample can easily be observed in Figure 11b. The pore pressure increases during this experiment all the way to the critical state point (Figure 11c). The critical state condition was achieved at point d in Figure 11a, at point e in Figure 11b, and at point F in Figure 11c.

Figure 12 shows a series of stress-strain curves for the deformation of sand at various confining pressures. A total of eleven experiments are shown. All the samples with effective confining pressures above 3400 psi show liquefaction behavior (as evidenced by the softening in the stress-strain curves) except for one test which had a jacket leak.

At this point some generalizations can be made about the process of liquefaction. Physical factors which are required for liquefaction to occur in sand include:

1) An undrained condition - the sand must have or be able to develop abnormally high fluid pressures. So, geologically sealing barriers must be present to trap pore fluids and to maintain the high pore pressures over time.

2) Prescence of shear stresses – sands undergoing hydrostatic deformation do not liquify no matter what the state of abnormal pore pressure.

3) High external bounding mean pressures – low mean pressures sands work harden and do not exhibit a runaway instability. At high mean pressures the sample can compress and pore pressures can build up leading to a reduction in the effective stresses.

4) Load control – In the natural setting the runaway instability must be induced by a condition where the applied bounding stresses can be continually maintained. In the laboratory this would be 'load' control as opposed to a displacement control.

5) Fully saturated – If the sand is fully fluid saturated, as opposed to gas saturated or partially saturated, then the development of liquefaction is favored.

The appearance and behavior of the stress-strain and the pore pressure curves are similar in morphology to those exhibited by high porosity sands tested in soil mechanics research. The only difference is that the deformational behaviors are occurring at much higher stress conditions than those observed in soil mechanics.

Selecting the Jacketing Material for Triaxial Experiments

Studying the deformational behaviors of weak, unconsolidated sands at high pressures presents the experimentalist with a series of interesting challenges. First, and foremost among these is the problem of selecting suitable jacketing materials to encase the samples during triaxial tests.

Several important considerations for selecting the jacket type include:

1) The material should be strong enough to keep out the confining fluid and be able to withstand extremely high distortional strains without rupturing.
2) The jacket should not significantly affect the strength of a weak unconsolidated sand sample. If care is not taken to insure that the jacket strength does not affect the overall deformational strength of the sample then the experimental results may not be valid. The jacket strength may not only alter the sample strength, but could also significantly change the elastic properties and the type of deformational behavior (e.g., brittle versus ductile) of the sample.
3) The jacket should have a surface to which sensors can be attached (e.g., acoustic sensors and shear wave bender elements) and is smooth enough for the free movement of features such as extensometer chains (which are part of the devices to measure circumferential strain).
4) The jacket material should be chemically non-reactive to both the pore fluid and the confining fluid.

In rock mechanics triaxial experiments jacketing materials, such as viton rubber, buna-N rubber, or heat shrinkable plastic materials such as polyolefin or teflon are used to seal the sample from the confining pressure conditions of from 200 to 20,000 psi. The jackets are strong enough to maintain seal integrity to prevent the confining fluid (generally oil) from leaking and contaminating the pore fluid (if saturated) and/or the rock. Soil mechanics triaxial tests are conducted at confining pressures of only 0 to 100 psi with water as a confining medium and thin latex membranes used as jackets. So the first step in determining the strength of the sands at high confining pressures was to determine which jacketing material to utilize. A series of unconfined tests were conducted on latex rubber, buna-N rubber, polyolefin, and teflon jackets. Figure 13 shows the results of such experiments on a cast NX-size sample (2.125 inch diameter by 4.25 inch length) of 3010 rubber. This rubber sample was loaded in unconfined compression both with and without each of the jackets to see if the jacket resisted lateral expansion of the sample. Evidence that this was occurring would be from a higher loading stress at given strain

level. The results clearly indicate that the best jacketing material would be the thin latex membrane (used in soil mechanics) with the buna-N exhibiting a slightly higher effect than the latex and with the polyolefin, and teflon each successively exhibiting a much higher strength effect. The polyolefin and teflon were both deemed unacceptable for testing unconsolidated sand samples as they altered both the strength and the Young's modulus and Poisson's ratio of the rubber standard. The buna-N rubber and latex shifted the initial strength of the sample by only about 10 psi and did not affect the Young's moduli and only slightly affected the Poisson's ratio of the rubber standard.

The latex rubber and buna-N rubber jackets would seem to be the most promising jackets for use on the unconsolidated sands. The latex was initially thought to be too unstable to use at high confining pressures. A ruptured membrane would result in sand being distributed throughout the pressure cell – a factor which can permanently damage the steel threads rendering the cell useless. (Note: Pressure lines and pressure intensifiers can be protected by filters. It is protection of the triaxial cell which in paramount in this case). Therefore the initial triaxial tests on dry sand (Figure 14) were conducted with buna-N rubber sleeves which had a wall thickness of 3mm.

However, a comparison with dry sands using latex and buna-N indicated that the buna-N significantly affected the strength of the dry sand (Figure 14). Given this observation the experimental staff decided to spend time in testing, with extreme care, the suitability of the use of latex membranes at high confining pressures. These membranes have a wall thickness of only 0.4 mm and are extremely flexible but have the disadvantage of decomposing due to reactions with the confining fluid (mineral oil). During testing it was determined that the latex membranes could maintain their integrity to confining pressures of 10000 psi for at least 3 hours if the grain size was around .2 mm (which deemed sufficient for our planned testing program).

Some of the sand samples were deformed to very high axial strains (~20%). The extreme barreling of the sample and the high axial shortening causes the flexible jackets to 'wrinkle' and fold to accommodate the strains. Again the flexible latex seemed to minimize the effects of this process more than either of the thicker jackets.

REFERENCES

Alberty, M.W. 2000. Shallow water flows: A problem solved or a problem emerging, *Offshore Technology Conference 2000*, OTC Paper 11971, pp. 67-73.

Abousleiman, Y. & Ghassemi, A. 1992. Laboratory determination of poroelastic parameters, Part I, Biot's effective stress, University of Oklahoma RMI Consortium Report RMC 92-12.

Abousleiman, Y. & Cheng, A. 1993. Anisotropic poroelasticity with applications, University of Oklahoma RMI Consortium Report RMC 93-19. 36p.

Abousleiman, Y. & Cheng, A. 1996. Mandel's problem revisited, in *Geotechnique* 46, No. 2, pp. 197-195.

Abousleiman, Y., Chhajlani, R., & Roegiers, J-C. 1994. Effect of stress variation on Biot's parameter, in First North American Rock Mechanics Symposium, Poster Session Abstracts, pp. 1-4.

Abousleiman, Y. & Cui, L. 2001. The theory of anisotropic poroelasticity with applications, In *Modeling in Geomechanics*, Zaman, M., Gioda, G., and Booker, J., pp. 561-593.

Amadei, B. 1983. *Rock anisotropy and the theory of stress measurements*, Springer-Verlag, 478p.

Aoki, T., Tan, C.P., & Bamford, W.E. 1993. Effects of deformation and strength anisotropy on borehole failures in saturated shales, *Int. J. Rock Mech. Min. Sci. & Geomech. Abstr.*, Vol. 30, No. 7, pp. 1031-1034.

Biot, M.A. & Willis, D.G. 1957. The elastic coefficients of the theory of consolidation, *J. of App. Mech*., Paper 57, pp. 594-601.

Carroll, M.M. 1979. An effective stress law for anisotropic elastic deformation, in *J. Geophy. Res*., Vol. 84, No. B13, pp. 7510-7512.

Cheng, A.H.-D. 1997. Material coefficient of anisotropic poroelasticity, *Int. J. Rock Mech. Min. Sci.& Geomech. Abstr*. , 34, pp 199-205.

Cui, L., Cheng, H.D., Kaliakin, V.N., Abousleiman, Y. & Roegiers, J.-C. 1996. Finite element analysis of anisotropic poroelasticity: A generalized Mandel's problem and an inclined borehole problem*, Int. J. for Numer. and Analyt. Meth. in Geomech.,* Vol. 20, pp. 381-401.

Fabre, D. & Gustkiewicz, J. 1998. Influence of rock porosity on Biot's coefficient, in *Poromechanics*, Thimus (ed.), pp. 561-566

Fatt, I. 1959. The Biot-Willis elastic coefficients for a sandstone, Trans. AIME, June, 1959, pp. 296-297.

Faul, R., Reddy, B.R., Griffith, J., Fitzgerald, R., Waugh, B., 2000, Next-generation cementing systems to control shallow water flow, Offshore Technology Conference 2000, OTC Paper 11977, pp. 117-122.

Fjaer, E., Holt, R.M., & Raaen, A.M. 1989. Rock mechanics and rock acoustics, *in Rock at Great Depth*, V. Maury and Fourmaintraux (eds.), pp. 355-362.

Franquet, J.A. & Abass, H.H. 1999. Experimental evaluation of Biot's poroelastic parameter – Three different methods, in *Rock Mechanics for Industry*, Amadei, Kranz, Scott, and Smeallie (eds.), pp. 349-355.

Furlow, W. 1998. Shallow water flows: how they develop; what to do about them, *Offshore,* September, p. 70.

Huffman, A. and Castagna, J.P. 2000, Shallow water flow prediction from seismic analysis of multicomponent seismic data, Offshore Technology Conference 2000, OTC Paper 11974, pp. 99-107.

Jones, L.E.A. & Wang, H.F. 1981. Ultrasonic velocities in Cretaceous shales from the Williston basin, *Geophysics*, v. 46, 3, p. 288-297.

King, M.S. 1969. Static & dynamic elastic moduli of rocks under pressure, in Somerton, W.H. (ed.) *Rock Mechanics-Theory and Practice: Proceedings 11th U.S. Symposium on Rock Mechanics*, p. 329-351.

King, M.S., Andrea, M., & Shams Khanshir, M., 1994. Velocity anisotropy of carboniferous mudstones, *Int. J. of Rock Mech. Min. Sci. & Geomech. Abstr.,* v. 31, 3, p. 261-263.

Laurent, J., Bouteca, M.J., Sarda, J.-P., & Bary, D. 1993. Pore-pressure influence in the poroelastic behavioir of rocks: Experimental studies and results, in *SPE Formation Evaluation*, June 1993, pp. 117-122.

Lo, T., Coyner, K.B., & Toksoz, M.N. 1986. Experimental determination of elastic anisotropy of Berea sandstone, Chicopee shale, and Chelmsford granite, *Geophysics*, v. 51, 1, p. 164-171.

McConnell, D.R. and Campbell, K.J. 1999. Interpretation and identification of potential shallow water flow from seismic data. Conference proceedings, 1999 International Forum on Shallow Water Flows, October 6-8, 1999.

McConnell, D.R. 2000. Optimizing deepwater well locations to reduce the risk of shallow-water flow using high-resolution 2D and 3D seismic data, Offshore Technology Conference 2000, OTC Paper 11973, pp. 87-97.

Nelson, R.A. 1981. A discussion of the approximation of subsurface (burial) stress conditions in laboratory experiments, *in Mechanical Behavior of Crustal Rocks*, Carter, Friedman, Logan, and Stearns (eds.), pp. 311-321

Nur, A. & Simmons, G. 1969. Stress-induced velocity anisotropy in rock: an experimental study, *Journal Geophysical Research*, v. 74, 27, p. 6667-6674.

Podio, A.L., Gregory, A.R. & Gray, K.E. 1968. Dynamic properties of dry and water saturated Green River Shale under stress, *Transactions Society of Petroleum Engineers of AIME*, v. 243, Sec. II, p. 389-404.

Sayers, C.M. & van Munster, J.G. 1991. Microcrack-induced seismic anisotropy of sedimentary rocks, Journal of geophysical research, Vol. 96, No. B10, pp 16,529-16,533.

Schofield, A.N. and Wroth, C.P. 1968. Critical state soil mechanics, McGraw-Hill: London, England.

Scott, Jr., T.E. Ma, Q. & Roegiers, J.-C. 1993. Acoustic velocity changes during shear enhanced compaction of sandstone*, Int. J. Rock Mech. Min. Sci. & Geomech. Abstr*., Vol. 30, No. 7, pp. 763-769.

Scott, Jr., T.E. & Abousleiman, Y. 2001. A method for measuring anisotropic Biot's parameters from acoustic wave propagation, EOS trans. Spring Meeting of the American Geophysical Union.

Scott, Jr., T.E. & Abousleiman, Y. 2002. Determination of the stress-induced dynamic moduli of a porous medium subjected to various deformational pathways, submitted to the Second Biot Conference on Poromechanics.

Thompson, M. & Willis, J.R. 1991. A reformation of the equations of anisotropic poroelasticity, Trans. ASME, Vol. 58, pp. 612-616.

Vaid, Y.P., and Eliadorani, A. 1998. Instability and liquefaction of granular soils under undrained and partially drained states, *Can. Geotech. J.*, 35, pp. 1053-1062.

Wang, Z.Z. 2001. Seismic anisotropy in sedimentary rocks. In 2001 SEG extended abstracts.

Wu, B., King, M.S., & Hudson, J.A. 1990. Stress-induced ultrasonic wave velocity anisotropy in a sandstone, p. 101-107.

LIST OF ACRONYMS AND ABBREVIATIONS

AE	=	Acoustic Emission
GAIS	=	Geomechanical Acoustic Imaging System
OU	=	The University of Oklahoma
RMI	=	Rock Mechanics Institute at the University of Oklahoma
SIRT	=	Simultaneous Iterative Reconstruction Technique
SWF	=	Shallow Water Flows
VHF	=	Very High Frequency
V_p	=	Compressional Wave Velocity
V_s	=	Shear wave velocity
V_p/V_s	=	Ratio of compressional wave velocity to the shear wave velocity

Project month	1	2	3	4	5	6	7	8	9	10	11	12	13	14	15	16	17	18	19	20	21	22	23	24
Task 1																								
Obtain Rock Samples	X	X																						
Task 2																								
Construct New Acoustic	X	X																						
Platens																								
Task 3																								
Calibrate Equipment	X	X																						
Task 4																								
Prepare Sandstone &		X	X	X																				
Chalk Samples																								
Task 5																								
Construct Lateral Acoustic		X	X	X																				
Sensors																								
Task 6																								
Reconnaissance Test				X	X	X																		
Chalk & Sandstones																								
Task 7																								
AE Hypocentral Location							X	X	X	X	X													
& Full Dynamic Tensor																								
Task 8																								
Correlate Static & Dynamic											X	X												
Parameters																								
Task 9																								
Test Sand Pack Samples													X	X	X									
Task 10																								
Ultrasonic Tomography on																X	X	X	X	X				
Sandstone & Chalks																								
Task 11																								
Make Deformation Velocity																					X	X		
Maps																								
Task 12																								
Final Report																							X	X

Table 1: Project time line with fifth quarter targets highlighted

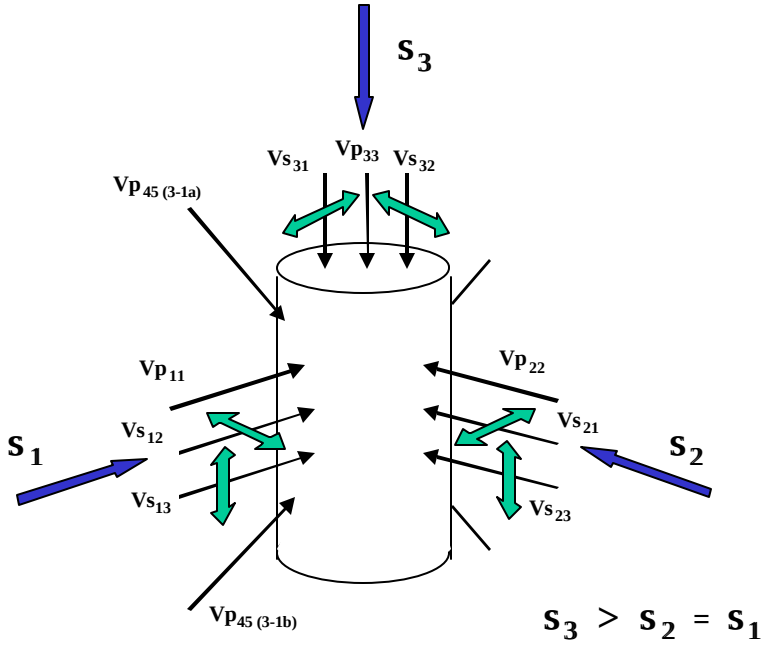

Figure 1. Three-dimensional orientation of acoustic raypaths on the cylinder core samples.

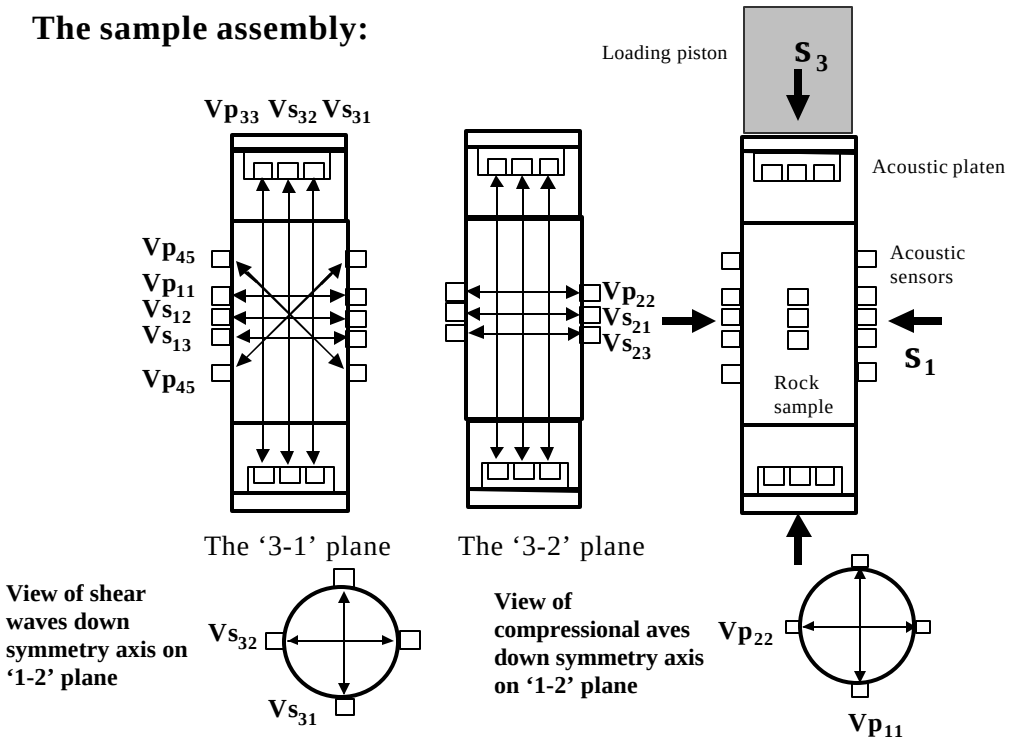

Figure 2. The experimental setup illustrating the acoustic raypaths through the cylindrical sample.

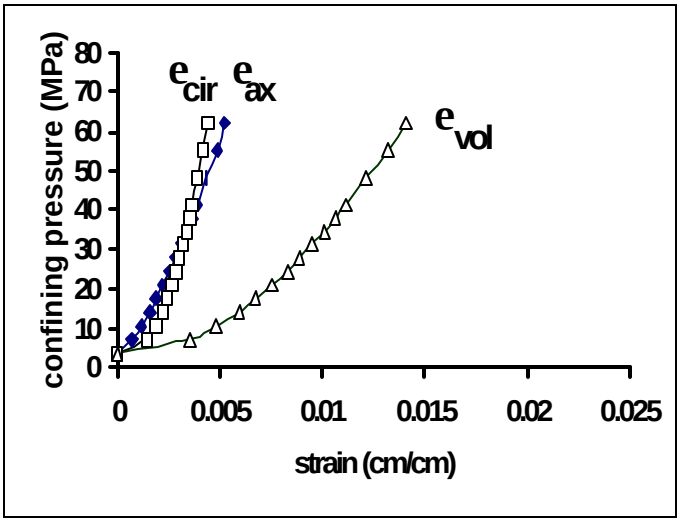

Figure 3a. The stress-strain curves for the hydrostatic experiment.

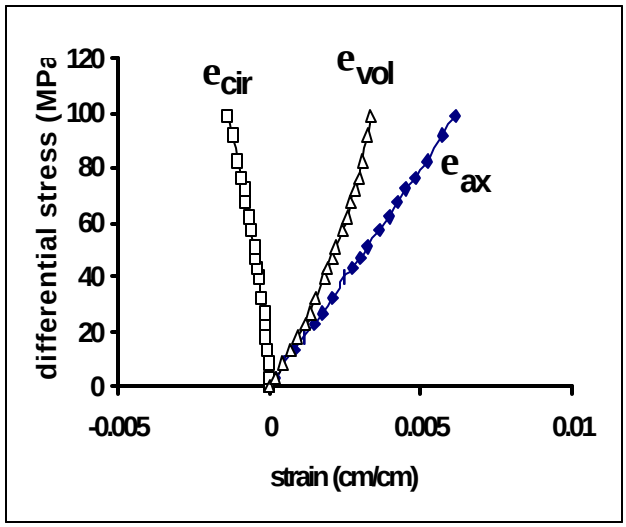

Figure 4a. The stress-strain curve for the triaxial compression experiment at 20 MPa confining pressure.

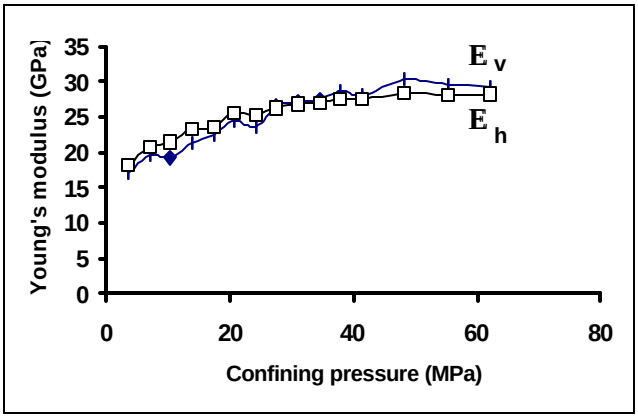

Figure 3b The axial and lateral Young's moduli during the hydrostatic experiment.

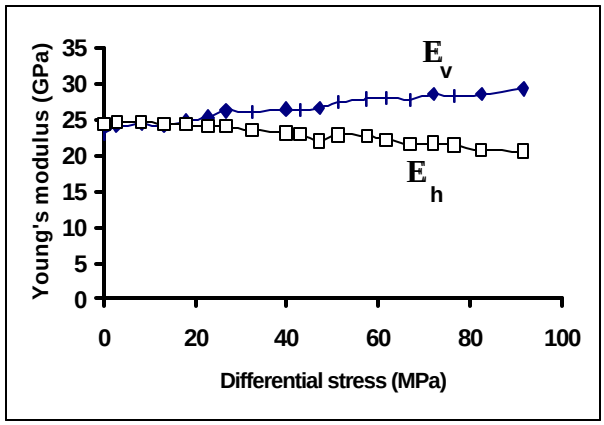

Figure 4b. The anisotropic Youngs moduli developed during the triaxial compression experiment..

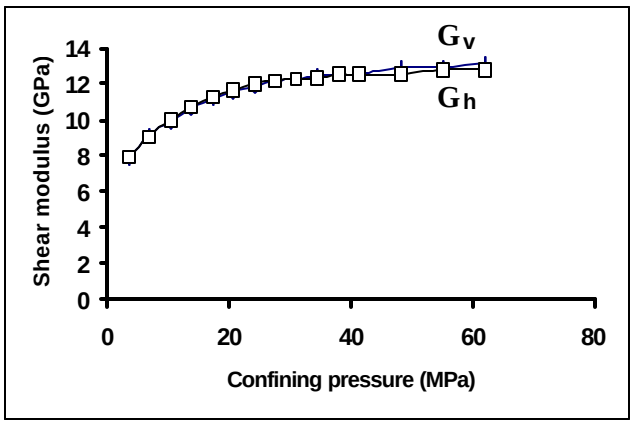

Figure 3c. The axial and lateral shear moduli for the hydrostatic experiment.

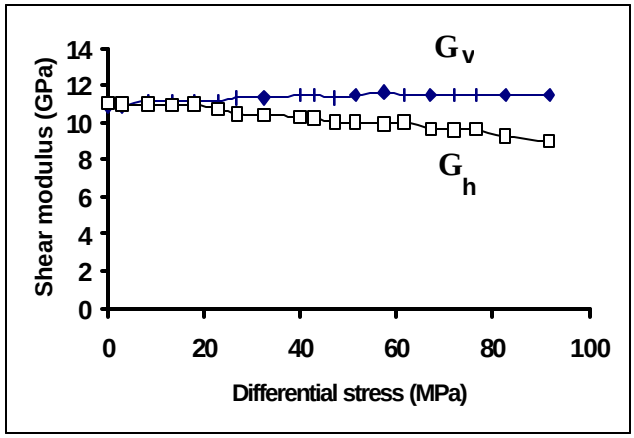

Figure 4c. The anisotropic shear moduli developed during the triaxial compression experiment.

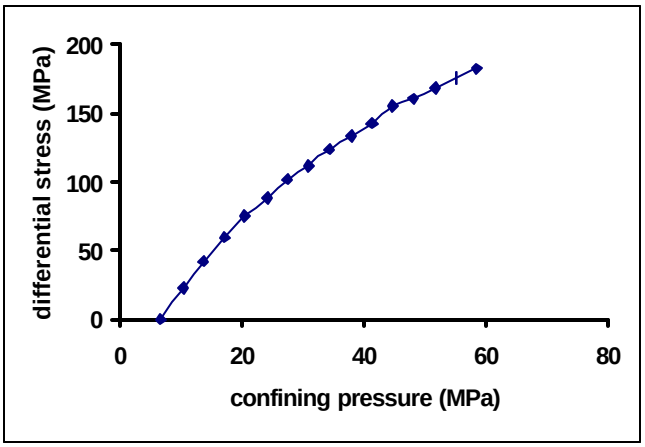

Figure 5a. Differential stress-confining pressure path for the uniaxial strain experiment.

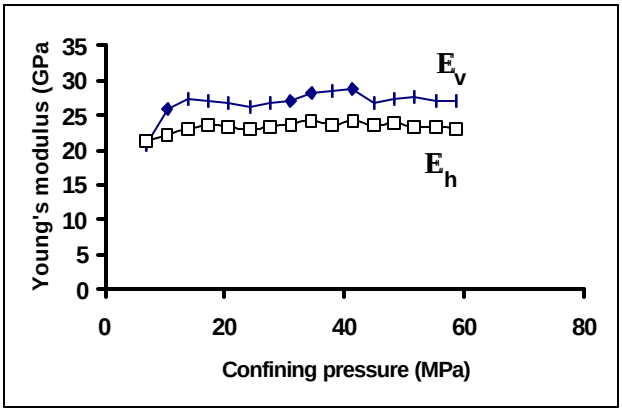

Figure 5b. A plot of the anisotropic Young's moduli during the uniaxial strain experiment.

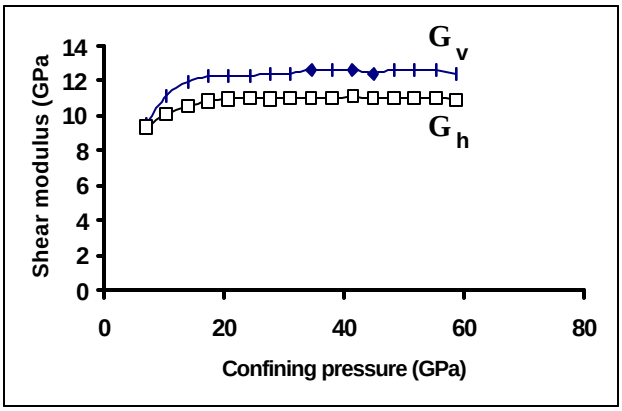

Figure 5c. A plot of anisotropic shear moduli developed during the uniaxial strain experiment.

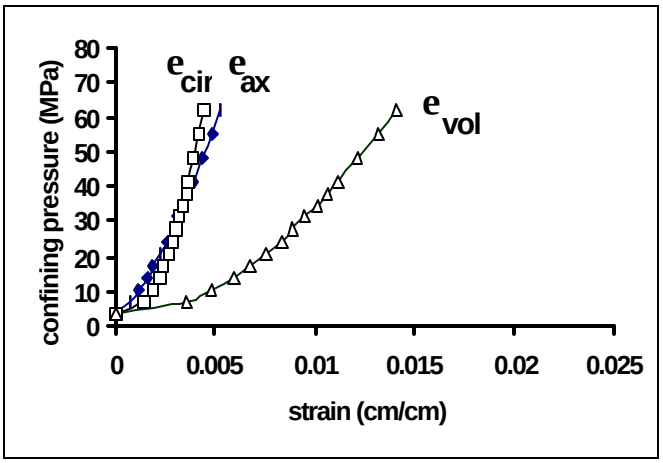

Figure 6a. Stress-strain curves for the hydrostatic experiment.

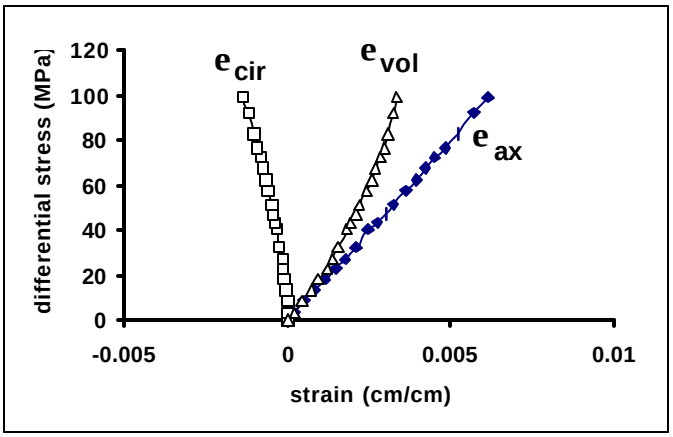

Figure 7a. Stress-strain curves for the triaxial compression experiment at 20 MPa confining pressure.

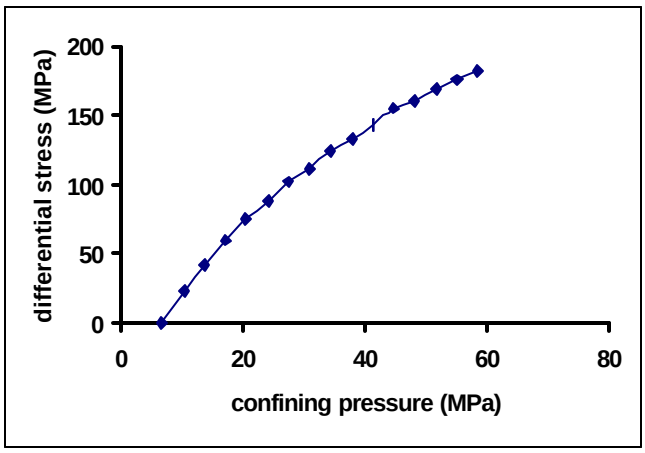

Figure 8a. The differential stress-confining pressure pathway for the uniaxial strain experiment starting at 6.9 MPa confining pressure.

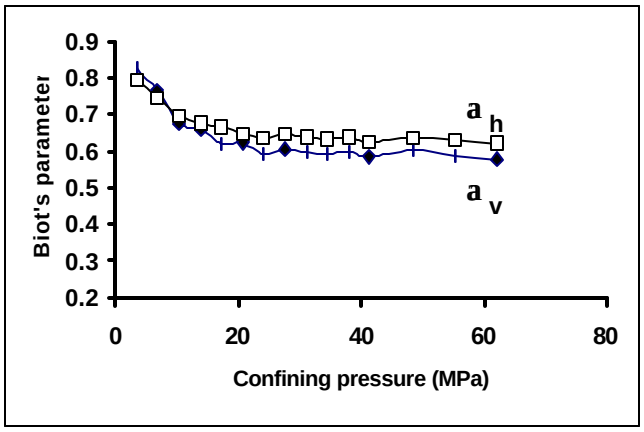

Figure 6b. A plot of Biot's parameter versus confining pressure during the hydrostatic experiment.

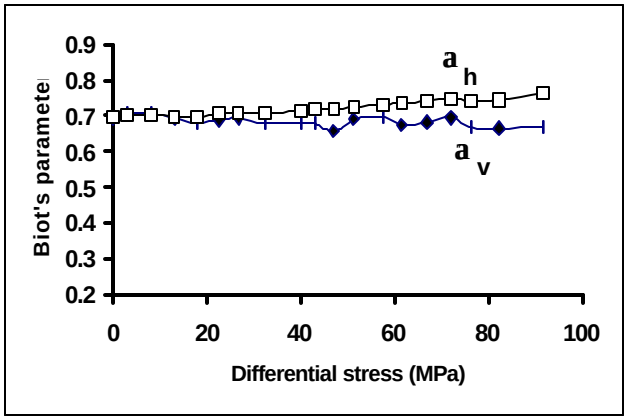

Figure 7b. A plot of anisotropic Biot's parameters versus differential stress during the triaxial compression experiment at 20 MPa confining pressure.

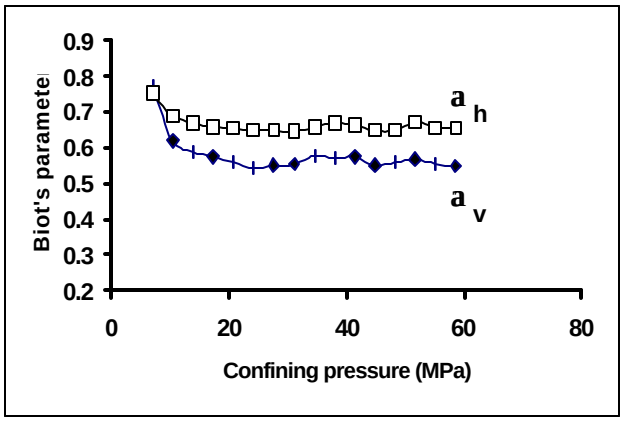

Figure 8b. A plot of the anisotropic Biot's parameters developed during a uniaxial strain experiment initiated at 6.9 MPa confining pressure.

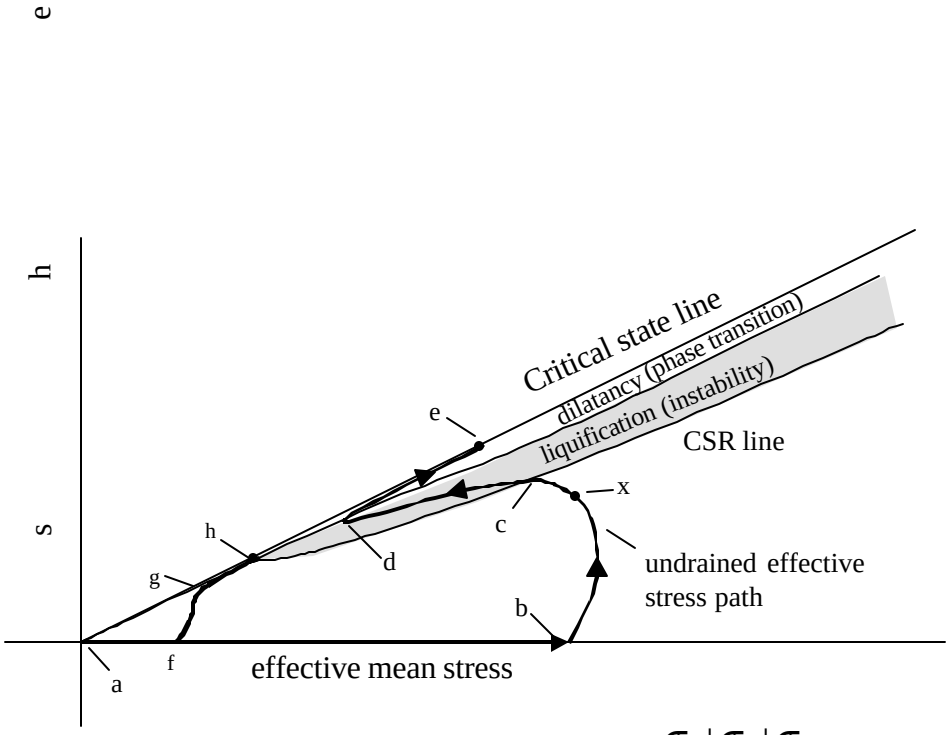

$$\text{mean stress} \quad P_m = \frac{\sigma_1+\sigma_2+\sigma_3}{3}$$

$$\text{effective mean stress} \quad P' = P_m - P_p$$

$$\text{shear stress} \quad q = \frac{\sigma_1 - \sigma_3}{2}$$

Figure 9. A schematic of the types of deformational pathways for undrained triaxial experiments in unconsolidated sands. The basic concept has been modified from Vaid and Eliadorani (1998).

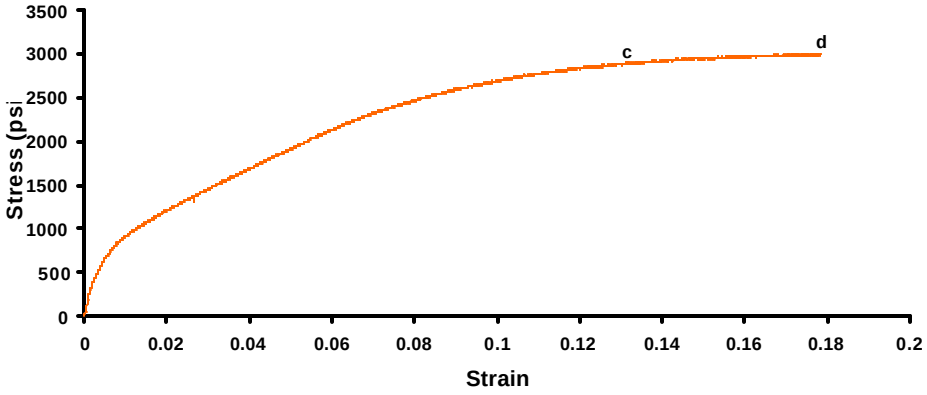

Figure 10a. The stress-strain curve for an undrained triaxial compression experiment at 2000 psi confining pressure and 1000 psi starting pore pressure.

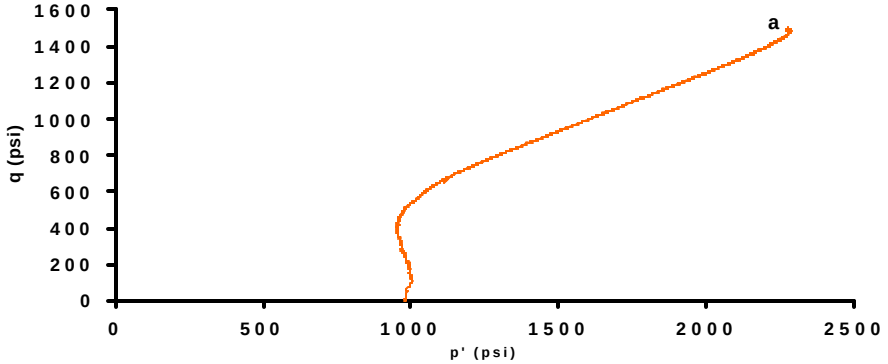

Figure 10b. The shear stress (q) versus effective mean pressure (p′) plot for an undrained triaxial compression experiment at 2000 psi confining pressure and 1000 psi starting pore pressure.

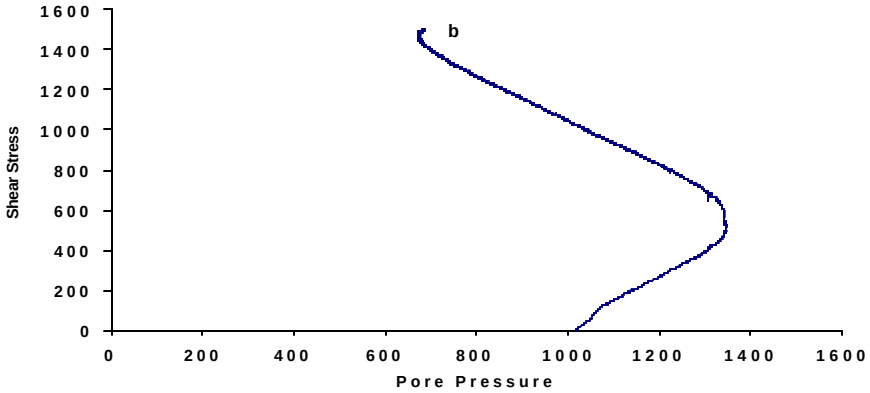

Figure 10c. The shear stress (q) versus pore pressure plot for an undrained triaxial compression experiment at 2000 psi confining pressure and 1000 psi starting pore pressure.

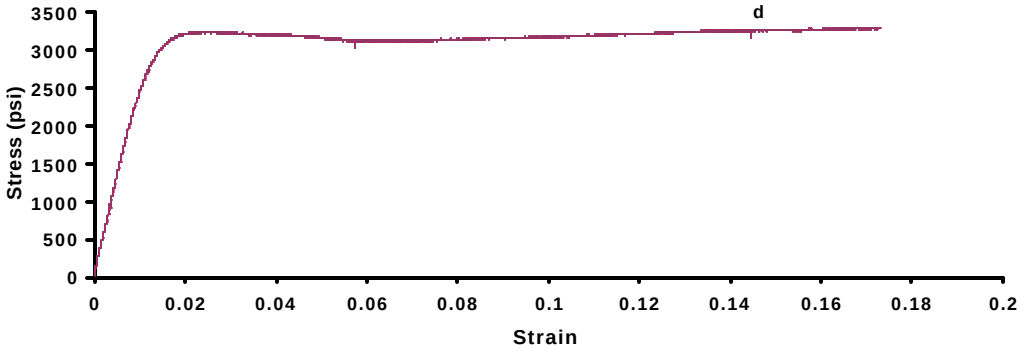

Figure 11a. The stress-strain curve for an undrained triaxial compression experiment at 5500 psi confining pressure and 600 psi starting pore pressure.

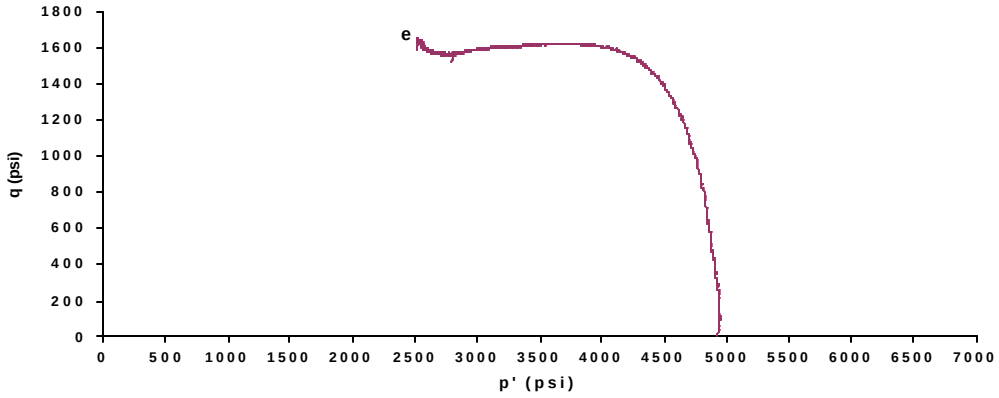

Figure 11b. The shear stress (q) versus effective mean pressure (p′) plot for an undrained triaxial compression experiment at 5500 psi confining pressure and 600 psi starting pore pressure.

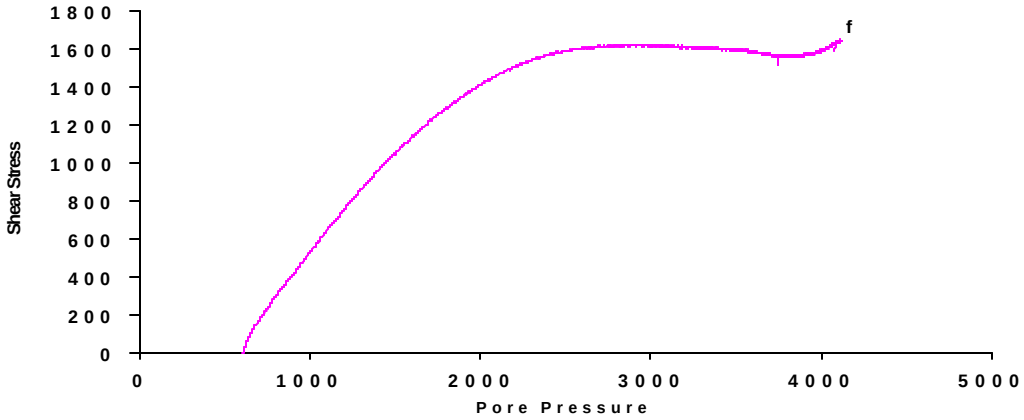

Figure 11c. The shear stress (q) versus pore pressure plot for an undrained triaxial compression experiment at 5500 psi confining pressure and 600 psi starting pore pressure.

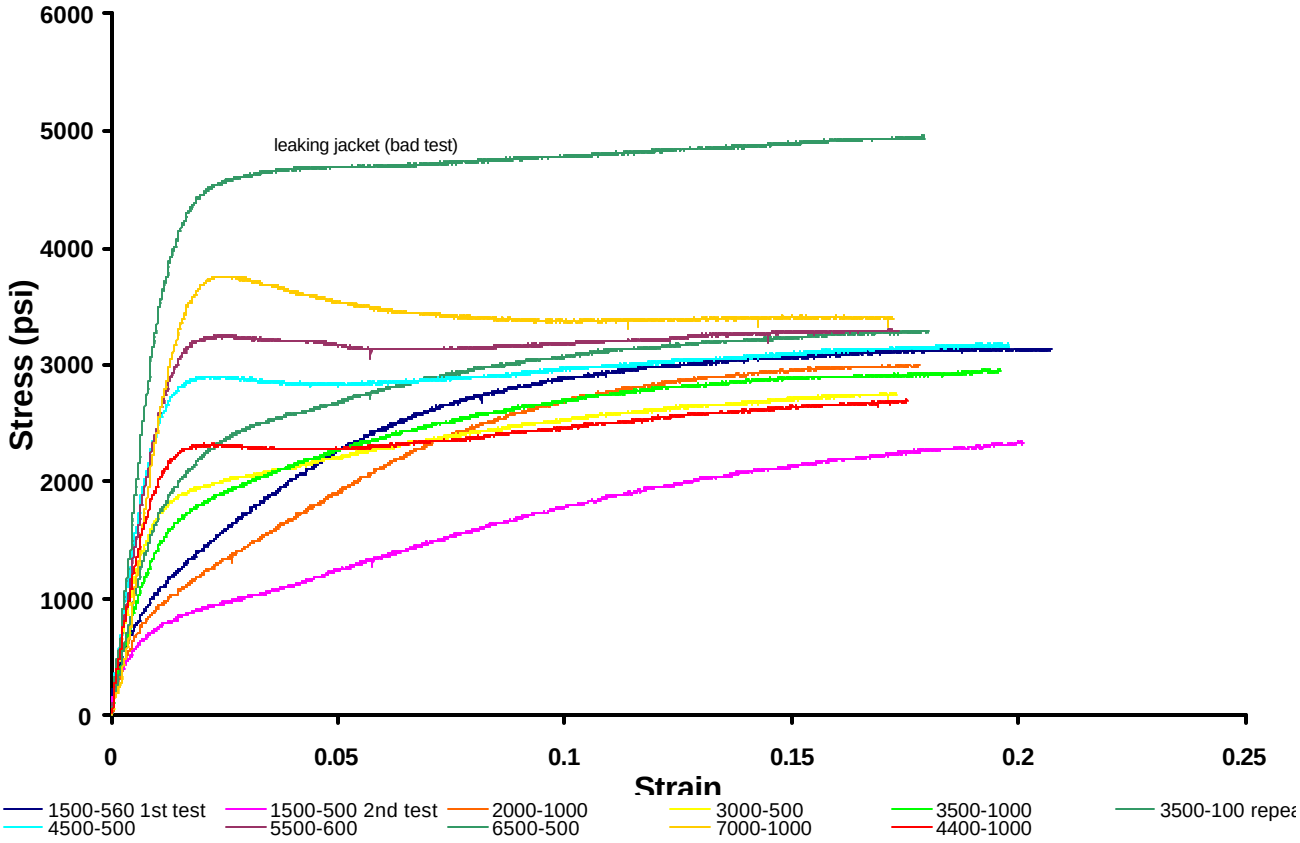

Figure 12. Stress-strain plots on a series of undrained triaxial compression experiments on unconsolidated Oil Creek sand. The first numbers of the legend represent the confining pressure and the second number is the starting pore pressure.

1

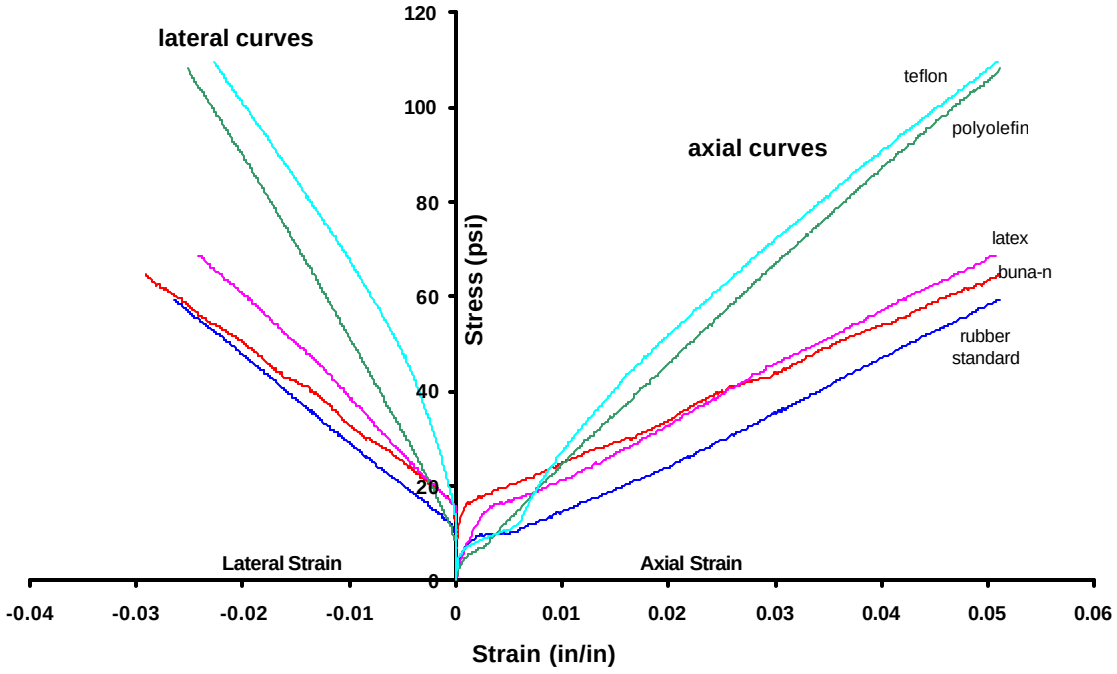

Figure 13. A comparison of the strength effect of various types of jacket types on a rubber standard.

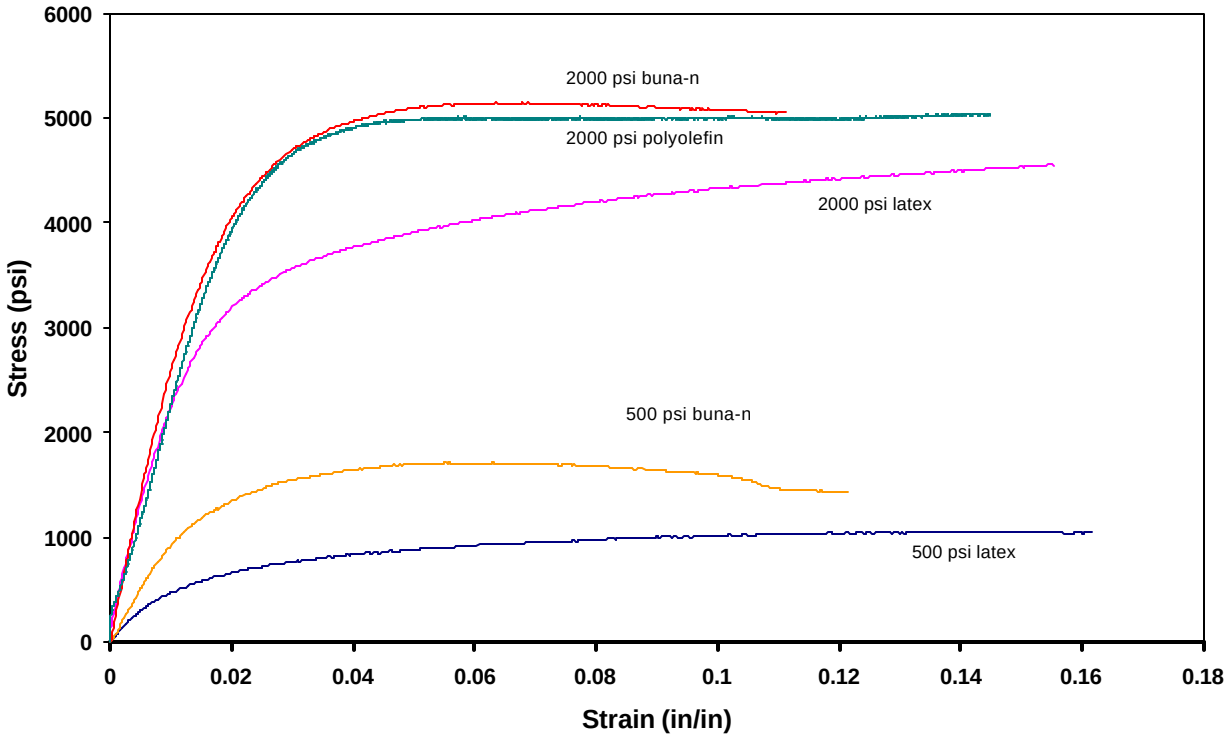

Figure 14. A comparison of jacket strength effects on the deformation of unconsolidated sand (Oil Creek sand).